ISSN (Print) 1226-1750
ISSN (Online) 2233-6656
Journal of Magnetics 21(4), 496-502 (2016) https://doi.org/10.4283/JMAG.2016.21.4.496

Effect of La^{3+} and Ti^{4+} Ions on the Magnetic Properties of Barium Hexaferrite Powders Synthesized Using Sol-Gel Method

Emre Burak Ertuş[1,2]*, Serdar Yildirim[2,3,4], and Erdal Çelik[2,4,5]

[1]*KTO Karatay University, Materials Science and Nanotechnology Engineering, Konya, Turkey*
[2]*Dokuz Eylul University, Electronic Materials Production and Application Centre, Izmir, Turkey*
[3]*Dokuz Eylul University, The Graduate School of Natural and Applied Sciences, Izmir, Turkey*
[4]*Dokuz Eylul University, Department of Metallurgical and Materials Engineering, Izmir, Turkey*
[5]*Dokuz Eylul University, Department of Nanoscience and Nanoengineering, Izmir, Turkey*

(Received 7 October 2015, Received in final form 12 August 2016, Accepted 7 October 2016)

Doped and undoped barium hexaferrite powders ($BaFe_{12}O_{19}$, $Ba_{0.7}Ti_{0.3}Fe_{12}O_{19}$ and $Ba_{0.7}La_{0.3}Fe_{12}O_{19}$) were produced by the sol-gel method. The effects of substituting elements were studied in terms of the magnetic properties of barium hexaferrite powders. The magnetic properties were remarkably changed by the substitution of La^{3+} and Ti^{4+} ions for the Ba^{2+} ion and were accompanied by oxygen deficiency in the $BaFe_{12}O_{19}$. Coercivities (H_C) from 4200 to 5100 Oe, remanences (M_R) from 22 to 49 emu/g and saturation magnetizations (M_S) from 41 to 73 emu/g were obtained for different samples. The obtained results were discussed in detail.

Keywords : barium hexaferrite, sol-gel, magnetic properties

1. Introduction

Barium hexaferrite with hexagonal molecular structure has received considerable attention in the area of magnetic materials due to its desirable properties such as low production cost, high Curie temperature (720 K), high coercive force, high saturation magnetization, magneto-crystalline anisotropy along c-axis, chemical stability, and corrosion resistance. These various properties have made barium hexaferrite potentially important in high-density perpendicular recording media, electromagnetic interference, magnetic fluids, microwave devices, sensors, microwave absorbing materials, ceramic magnets in loud speakers, and the rotors in DC motors. It is known that the magnetic properties of $BaFe_{12}O_{19}$ powders vary with substituting (doping) elements, grain size, purity, production method, and annealing/sintering conditions (temperature and time) [1-5].

Various chemical routes are employed to synthesize the micro and nano particles of barium hexaferrite: the conventional ceramic method, chemical co-precipitation, microemulsion, glass crystallization, combustion, sol-gel synthesis, hydrothermal synthesis, oxidation in nitric acid method, self-propagating high temperature synthesis, and the ammonium nitrate melt (ANM) technique. Among these methods, the sol-gel technique has significant advantages such as being simple, economic, and effective. The sol-gel process offers better mixing of the starting materials, more easily controllable composition and doping elements, low sintering temperatures, high purity and better crystallized final products [1-4].

The intrinsic magnetic properties of the barium hexaferrite can be changed by partial substitutions for Ba or Fe sites [6-12]. Previous works have shown that the magnetic properties of barium hexaferrite could be changed by substituting Ba^{2+} with rare earth ions [10, 13-15]. Li *et al.* [13] and S. Ounnukad [10] reported that the substitution of small amounts of La^{3+} ions increase the coercive force while decreasing the saturation magnetization. The aim of the present research is to synthesize pure and substituted barium hexaferrite ($BaFe_{12}O_{19}$, $Ba_{0.7}Ti_{0.3}Fe_{12}O_{19}$ and $Ba_{0.7}La_{0.3}Fe_{12}O_{19}$) with high substitution levels by means of the sol-gel method. Altering the magnetic properties of the barium hexaferrite material has great importance in applications like radar absorbing materials and sensors. In order to change the magnetic properties of barium hexaferrite, substituting ions like Lanthanum (La) and titanium (Ti) are chosen. There is a difference bet-

*Corresponding author: Tel: +90-5066262951
Fax: +90-332-202-00-44, e-mail: burakertus@gmail.com

ween the ionic radius of the base ion (Ba^{2+} = 149 pm) and the partial substituting ions (La^{3+} = 117 pm and Ti^{4+} = 74.5 pm) [16]. Substituting ions are expected to change the lattice parameters of $BaFe_{12}O_{19}$. This will cause lattice distortion and will change the atomic distances between the magnetic moment producing ions. Thus, the total magnetization and other magnetic properties will vary with substituting ions placed in the crystal lattice.

2. Experimental Procedure

In order to produce pure and well crystallized magnetic powders in the exact stoichiometry and without improper intermediate phases, homogenous solutions must be prepared. Barium nitrate $Ba(NO_3)_2$, iron (III) nitrate nonahydrate $Fe(NO_3)_3{\cdot}9H_2O$, lanthanum (III) nitrate hexahydrate $La(NO_3)_3{\cdot}6H_2O$, and titanium (IV) isopropoxide $C_{12}H_{28}O_4Ti$ are used as precursor materials. In addition, solvents are chosen as ethyl alcohol, isopropyl alcohol, and deionized water. The generalized solution preparation steps are summarized and shown in Fig. 1. The solution stoichiometries of undoped, La doped and Ti doped barium hexaferrite powders are listed in Table 1.

In the sol gel method, it is possible to obtain higher quality products by modifying some critical values of the production steps. In order to synthesize barium hexaferrite with fine-sized and best crystal structure, pH is increased and fixed at 10 by adding an ammonium hydroxide solution [17]. Citric acid is chosen as chelating agent. To synthesis single phase barium hexaferrite at relatively low temperatures the "Citric Acid/Total Metal Ions" molar ratio is adjusted to 2 [4]. By considering the poor solubility of Ba^{+2} cations in water, the molar ratio of Fe/Ba is 11 to maintain the stoichiometry of the product [18, 19].

The water in the prepared solution is gradually removed by heating at 80 °C for 10 hours in a water bath to obtain wet gel with high viscosity. Then the wet gel is heat treated at 180 °C for 2 hours in a drying oven until all the water evaporates. Next, the dry gel (xerogel) is exposed to the pre-sintering process at 500 °C for 30 minutes to remove all other impurities and organics like C, H, and N. After pre-sintering at 800 °C for 30 minutes, final sintering at 1,000 °C for 2 hours is applied for final phase transformation in the chamber furnace. All sintering steps are applied in the air atmosphere at the heating rate of 10 °C/min. The expected main chemical reactions associated

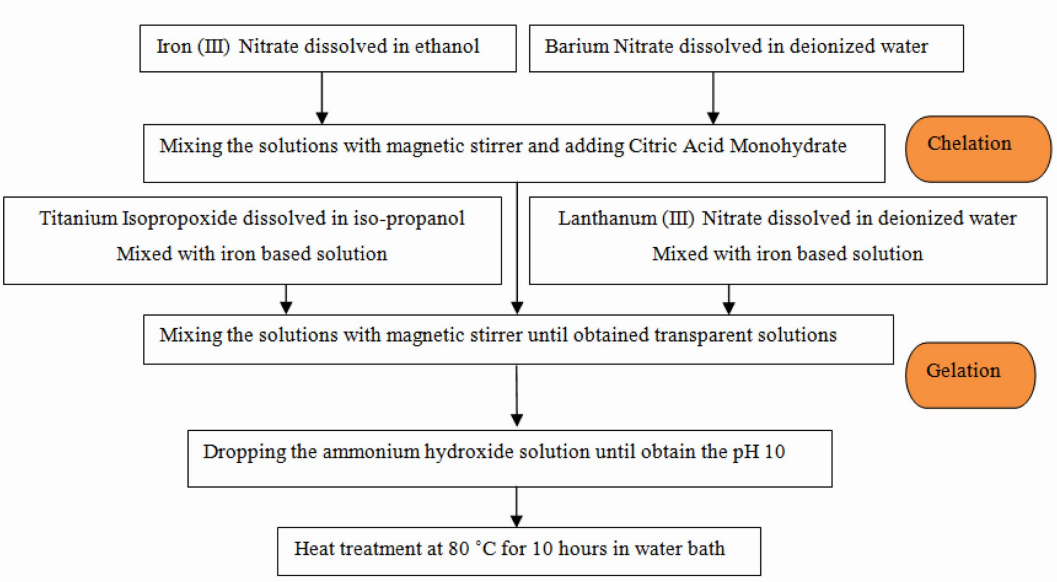

Fig. 1. (Color online) Solution preparation steps.

Table 1. Stoichiometric ratios of precursor elements in different solutions.

Solution type	Precursor element				Chelating agent
	Iron	Barium	Lanthanum	Titanium	Citric acid monohydrate
Undoped	11 mol	1 mol	-	-	24 mol
La Doped	11 mol	0.7 mol	0.3 mol	-	24 mol
Ti Doped	11 mol	0.7 mol	-	0.3 mol	24 mol

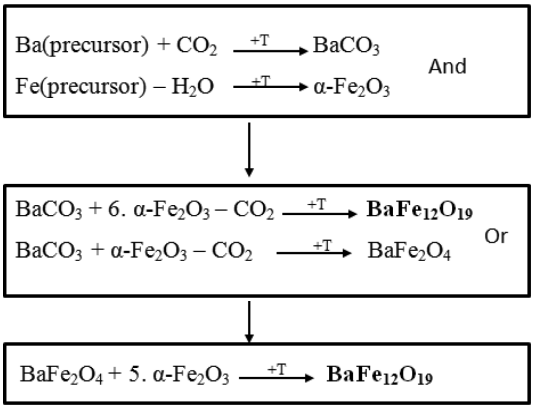

Fig. 2. Chemical reactions associated with the formation of the barium hexaferrite.

with the formation of the barium hexaferrite are summarized in Fig. 2 [20].

The fourier Transform Infrared (FTIR) absorption spectra of doped and undoped barium hexaferrite samples are recorded over the range of 4,000 to 650 cm^{-1} with Perkin Elmer Spectrum BX model FTIR equipped with an ATR apparatus to determine the chemical bonds and organic components in the samples. X-ray diffraction (XRD) patterns are determined by Thermo-Scientific, ARL-Kα. The scanning speed is 2°/min between 15º and 80º. Elemental analyses of barium hexaferrite powders are analyzed via X-ray photoelectron spectroscopy (XPS, Thermo-Scientific Al-Kα) especially to observe substituting elements in barium hexaferrite powders. Scanning electron microscopy (SEM) images are taken by JEOL JSM-6060 instrument to examine the morphology of the magnetic particles. Materials are examined under 10000X and 25000X magnifications at an accelerating voltage of 15 kV. Finally, the magnetic properties of barium hexaferrite powders are measured at room temperature by using a Vibrating Sample Magnetometer (VSM, Dexing Magnet Co.) with an applied field up to 11000 Oersted. The hysteresis loop, saturation magnetization (M_S), remanent magnetization (M_R) and coercivity (H_C) are determined by VSM analysis.

3. Results and Discussion

Figures 3 (a) and (b) show the FTIR spectra of $BaFe_{12}O_{19}$ powders heat treated at 180 °C and 1000 °C. In Fig. 3 (a), there are two strong bands observed for all samples heat treated at 180 °C. The peak, which was observed near 1650 cm^{-1} is related to the H-O-H bending vibration [18]. This peak has resulted from the water existing either as absorbed water or the water of hydration. Note that the absorption band 1450 cm^{-1} has resulted from the carbonate groups and carbonate intermediates like $BaCO_3$ and CO_3^{-2} anion. The reason of the absorbance intensity differences between samples is using different starting precursors and solvents. The characteristic absorption bands for $BaFe_{12}O_{19}$ appear at around 591 and 438 cm^{-1} according to the literature and the FTIR spectra libraries [21]. In our analysis we can see only the initial portion of

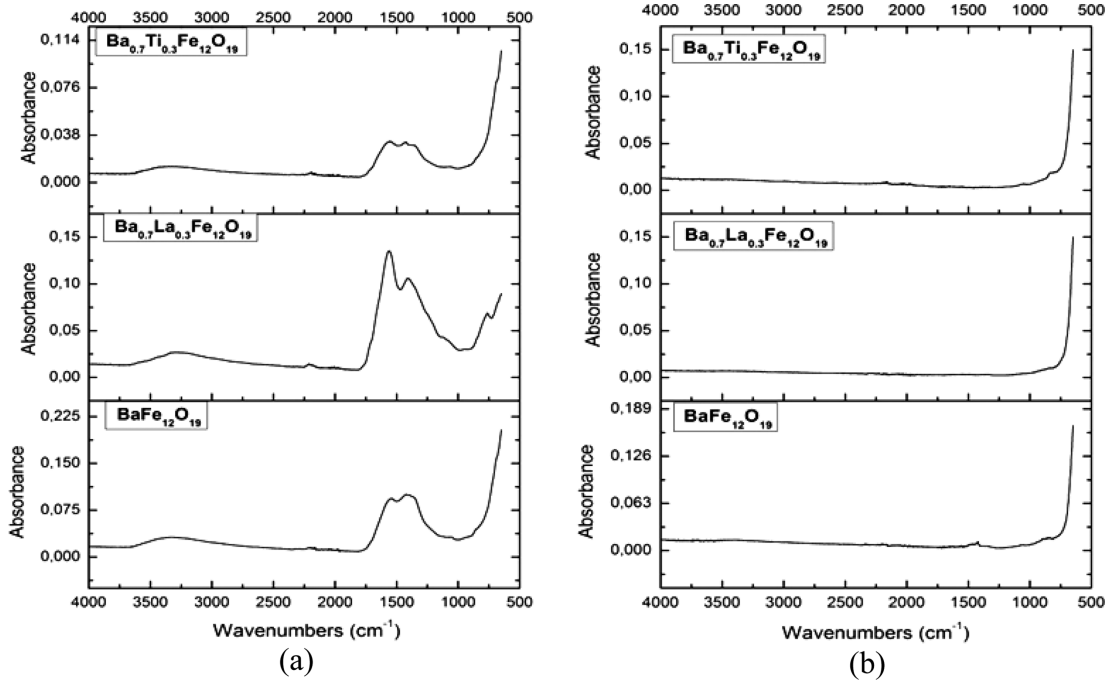

Fig. 3. FTIR analysis of barium hexaferrite samples after heat treatment at (a) 180 °C and (b) at 1000 °C.

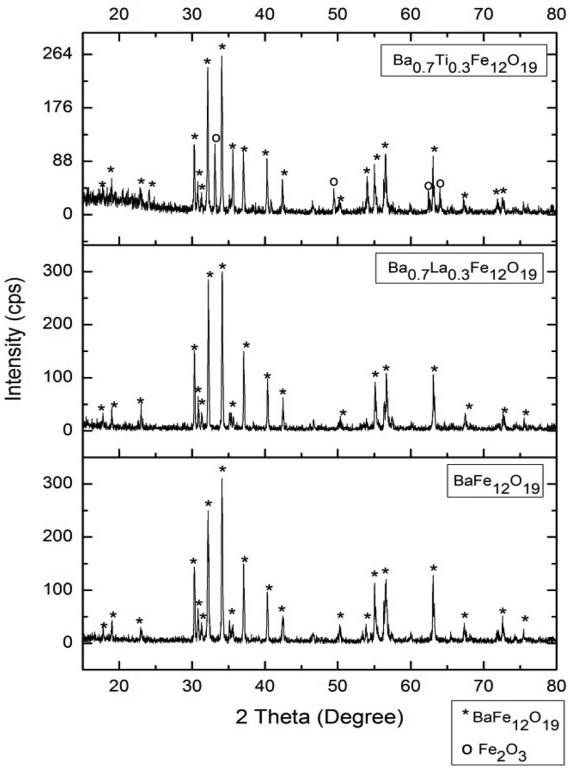

Fig. 4. XRD patterns of $BaFe_{12}O_{19}$, $Ba_{0.7}La_{0.3}Fe_{12}O_{19}$ and $Ba_{0.7}Ti_{0.3}Fe_{12}O_{19}$ samples heat treated at 1000 °C for 2 hours in air.

this absorption band peaks around 650 cm^{-1} since ATR apparatus works in the range of 650 cm^{-1} and 4000 cm^{-1}. After heating up to 1000 °C there is no sign of organics in Fig. 3 (b).

XRD patterns of undoped, Ti-doped and La-doped barium hexaferrite powders heat-treated at 1000 °C are represented in Fig. 4. The obtained patterns are compared in the device library using the search match operation. Clearly, barium hexaferrite became the major phase in samples $BaFe_{12}O_{19}$ and $Ba_{0.7}La_{0.3}Fe_{12}O_{19}$. It is evident that there is no mismatched or undefined peak. XRD patterns indicate that unreacted intermediate phases like barium monoferrite, ferrite and barium carbonate do not exist in these samples. In $Ba_{0.7}Ti_{0.3}Fe_{12}O_{19}$ sample, small amount of unreacted phase Fe_2O_3 is observed in XRD results. This might be resulted from Ti^{4+} ions block the structure sides or raise the final phase transition temperature. Thus Ba^{2+} ions could not diffuse to the desired crystal lattice positions. XRD patterns of all samples are in good agreement with FTIR analysis results. XRD studies suggest that the La^{3+} and Ti^{4+} ions have entered into the $BaFe_{12}O_{19}$ lattice because there wasn't any phase sign associated with these elements. The barium hexaferrite powders were well crystallized and widely matched with Powder Diffraction File (PDF no. 043-0002) reference patterns. For further investigation lattice parameters (a and c) and lattice volume were refined and calculated by using CMPR software [23]. As shown in Table 2 lattice parameters are changed with substituting elements. Both lattice constants and the lattice volume are

Table 2. Lattice constants (a, c) and lattice volume (V) of doped and undoped $BaFe_{12}O_{19}$ samples.

Sample	a (Å)	c (Å)	V (Å^3)
$BaFe_{12}O_{19}$	5.89056	23.18828	697.1077
$Ba_{0.7}La_{0.3}Fe_{12}O_{19}$	5.88771	23.14718	694.8978
$Ba_{0.7}Ti_{0.3}Fe_{12}O_{19}$	5.89341	23.22023	698.4416

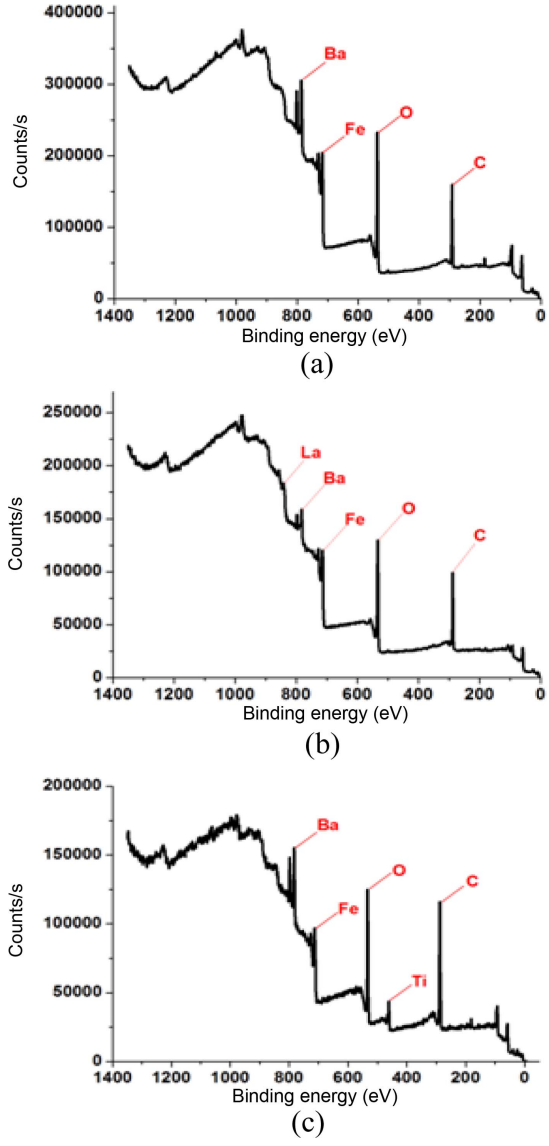

Fig. 5. (Color online) XPS analysis results of (a) $BaFe_{12}O_{19}$, (b) $Ba_{0.7}La_{0.3}Fe_{12}O_{19}$ and (c) $Ba_{0.7}Ti_{0.3}Fe_{12}O_{19}$ powders.

decreased in La doped sample, but they are increased in Ti doped sample although Ti^{4+} ion is smaller than Ba^{2+} ion. It should be considered that Fe_2O_3 peaks are observed in Ti samples, in this context, it can be said that some of Fe^{3+} ions placed in Fe_2O_3 lattice and there is Fe^{3+} deficiency in $BaFe_{12}O_{19}$ lattice. Increasing volume abnormality can be explained by Ti^{4+} ions filling the gaps of the Fe^{3+} ions where Fe^{3+} ions (63 pm) are smaller than Ti^{4+} (74.5 pm) ions.

The XPS analysis of barium hexaferrite powders are represented in Fig. 5. Ba, Fe, O and C elements are detected in all samples. The presence of Ba, Fe and O elements is an expected result and confirms the XRD results. Most likely the pollution on the samples causes the presence of Carbon element because XPS is a very sensitive device and the presence of carbon is often negligible. The remarkable part of the XPS analysis is the presence of La element in $Ba_{0.7}La_{0.3}Fe_{12}O_{19}$ sample and the presence of Ti element in $Ba_{0.7}Ti_{0.3}Fe_{12}O_{19}$ sample (see Figs. 5 (b) and 5(c) for details). If we consider both the XRD and the XPS analysis results it is clear that the substituting process is performed successfully. Dopant elements substituted crystal lattice parameters as required without generating undesirable phases or evaporation. In addition, all precursor metals which are used in the sol-gel process are observed in final product.

SEM images of $BaFe_{12}O_{19}$, $Ba_{0.7}Ti_{0.3}Fe_{12}O_{19}$ and $Ba_{0.7}La_{0.3}Fe_{12}O_{19}$ powders are represented in Fig. 6. Particle morphology is an important parameter which affects magnetic properties as mentioned before. It should be noted that the processing parameters such as stoichiometry, pH and heat treatment regime directly affect the powder morphology. Once the SEM images are analyzed, it indicates that the M-type barium hexaferrite particles are homogeneous hexagonal-shaped particles with a narrow distribution in particle size. The average particle size is observed about 430 nm for all samples. The major structure of particles is hexagonal and plate like shape but the La doped particles (see Fig. 6 (c) and (d)) have sharper edges. The Ti doped particles (Fig. 6. (e) and (f)) have more intergrain connectivity and some particles are in rod like shape. Also Ti doped particles have a little bigger grain sizes due to agglomeration of small particles. If we consider the XRD analysis results, it can be seen

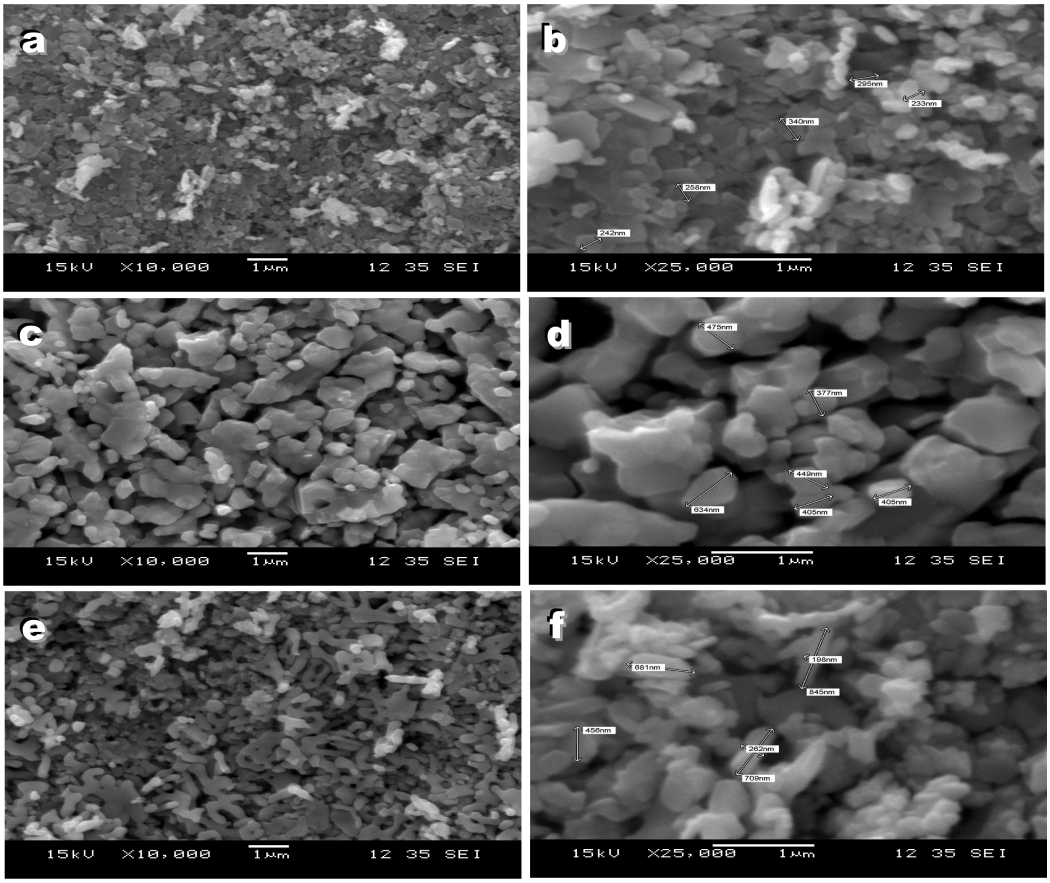

Fig. 6. SEM images of $BaFe_{12}O_{19}$ powders (a) 10000x (b) 25000x, $Ba_{0.7}La_{0.3}Fe_{12}O_{19}$ powders (c) 10000x, (d) 25000x and $Ba_{0.7}Ti_{0.3}Fe_{12}O_{19}$ powders (e) 10000x, (f) 25000x.

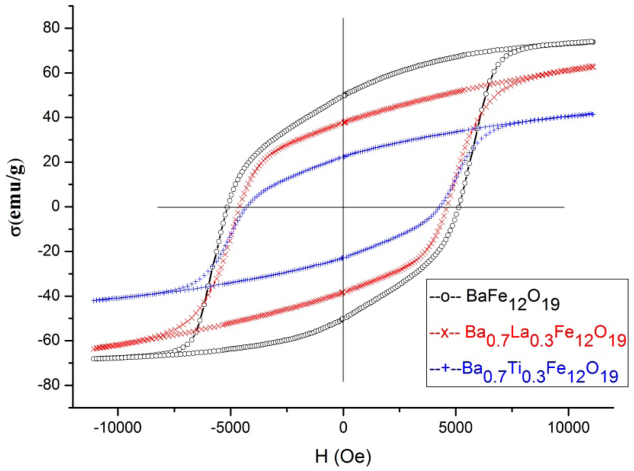

Fig. 7. (Color online) Hysteresis loops of $BaFe_{12}O_{19}$, $Ba_{0.7}La_{0.3}Fe_{12}O_{19}$ and $Ba_{0.7}Ti_{0.3}Fe_{12}O_{19}$ samples.

that lattice parameters of powders are changed with substituting. It can be expressed that the change in lattice parameters and lattice volume may be the cause of this change in microstructure.

Mass magnetization (M, σ, emu/g) versus magnetic field (H, Oe) curves (hysteresis loops) are obtained by VSM device with maximum magnetic field 11 kOe. The hysteresis loops of $BaFe_{12}O_{19}$, $Ba_{0.7}Ti_{0.3}Fe_{12}O_{19}$ and $Ba_{0.7}La_{0.3}Fe_{12}O_{19}$ samples are shown in Fig. 7. The magnetic properties of samples such as saturation magnetization M_S, remanent magnetization M_R and coercivity H_C values are listed in Table 3. Under applied magnetic field, all samples exhibit the hysteresis loops of the ferrimagnetic and hard ferrite nature. The examined results show that, La and Ti substituting led to decrease the magnetic properties of samples such as saturation magnetization M_S, remanent magnetization M_R and coercivity H_C. At this point, there are several valid reasons that can explain these changes in magnetic properties. First of all it should be remembered that the substituting ions are smaller than base ion so this might cause distortion in lattice parameters of $BaFe_{12}O_{19}$ [7, 10, 22]. Undoped sample possesses the largest coercive force (H_C) and the largest hysteresis loop area than doped ones. The main factor which may lead the larger hysteresis loss is strong uniaxial anisotropy along the c-axis. With the large amount of substitution, H_C decreases as a result of reduction in the crystal anisotropy field owing to the change of the easy-axis of magnetization from the c-axis to the basal plane. The moderately low H_C remarks that the domain wall motion becomes the dominant magnetization mechanism [22].

Table 3. Magnetic properties of $BaFe_{12}O_{19}$, $Ba_{0.7}La_{0.3}Fe_{12}O_{19}$ and $Ba_{0.7}Ti_{0.3}Fe_{12}O_{19}$ samples.

Sample	M_R (emu/gr)	M_S (emu/gr)	H_C (Oe)
$BaFe_{12}O_{19}$	49	73	5100
$Ba_{0.7}La_{0.3}Fe_{12}O_{19}$	37	63	4600
$Ba_{0.7}Ti_{0.3}Fe_{12}O_{19}$	22	41	4200

Distortion in crystal lattice parameters cause spin canting which means spins were tilted by a small angle about their axis rather than being exactly co-parallel where canted spin promotes lower M_S. The Fe^{3+}-O-Fe^{3+} superexchange interaction is disrupted and weakened as a consequence of the atomic distances between the magnetic moment producing ions anticipated to change [10, 11, 13]. Also note that there is partial transformation of Fe^{3+} to Fe^{2+} with substituting in order to compensate the excess positive charges due to the replacement of Ba^{2+} by La^{3+} or Ti^{4+} ions. The ionic magnetic moment of Fe^{2+} ions (ion magnetic moment is $4M_B$) are lower than the magnetic moment of Fe^{3+} ions (ion magnetic moment is $5M_B$). As a result, both M_R and M_S descend after La and Ti substituting [14, 15]. Furthermore Ti^{4+} ions distort lattice parameters much more and magnetic properties are lower than La^{3+} substituted samples.

4. Conclusions

To sum up, $BaFe_{12}O_{19}$, $Ba_{0.7}La_{0.3}Fe_{12}O_{19}$ and $Ba_{0.7}Ti_{0.3}Fe_{12}O_{19}$ magnetic powders are successfully produced via sol-gel method. After final phase transformation at 1,000 °C, it can be clearly seen from FTIR results that all organic materials were burnt out. XRD and XPS results show that the dopant elements substituted crystal lattice parameters as required without generating undesirable phases or evaporation. According to XRD results, $BaFe_{12}O_{19}$ phase was successfully obtained without any mismatched or undefined peaks. M-type barium hexaferrite particles are homogeneous hexagonal-shaped crystals, with a narrow distribution in particle size (around 430 nm) as observed in SEM images. The hexagonal and plate like shape is the major particle structure. Only Ti substituted particles have a little bigger sizes with rod like shape particles. The examined VSM results show that under applied magnetic field all samples exhibit the hysteresis loops of the ferrimagnetic and hard ferrite nature. La and Ti substituting led to decrease magnetic properties of samples such as saturation magnetization M_S, remanent magnetization M_R and coercivity H_C due to lattice distortion and partial transformation of Fe^{3+} to Fe^{2+}. As a result, the magnetic properties of barium hexaferrite can be tuned by substituting elements so it is an appropriate candidate to be used in applications like radar absorbing materials and

sensors.

Acknowledgements

This study was conducted as part of the Master of Science thesis in Dokuz Eylül University, The Graduate School of Natural and Applied Sciences. This research also was supported by TEKNOBIM Company, Izmir, Turkey. This was a KOSGEB project (Project No: 2011/30). The authors want to thank to the specialist engineers whose were very helpful at every stage of production and characterization processes of this study at Center for Production and Application of Electronic Materials (EMUM).

References

[1] R. C. Pullar, Prog. Mater. Sci. **57**, 1191 (2012).
[2] M. M. Rashad and I. A. İbrahim, J. Magn. Magn. Mater. **323**, 2158 (2011).
[3] M. Mozaffari, M. Taheri, and J. Amighian, J. Magn. Magn. Mater **321**, 1285 (2009).
[4] A. Mali and A. Ataie, Ceram. Inter. **30**, 1979 (2004).
[5] U. Topal and H. I. Bakan, J. Eur. Ceram. Soc. **30**, 3167 (2010).
[6] N. A. Spaldin, Magnetic Materials Fundamentals and Applications, Second Ed., Cambridge University Press, New York (2010) pp. 124-126.
[7] M. Jazirehpour, M. H. Shams, and O. Khani, J. Alloys Compd. **545**, 32 (2012).
[8] V. V. Soman, V. M. Nanoti, and D. K. Kulkarni, Ceram. Inter. **39**, 5713 (2013).
[9] V. N. Dhage, M. L. Mane, A. P. Keche, C. T. Birajdar, and K. M. Jadhav, Phys. B **406**, 789 (2011).
[10] S. Ounnunkad, Solid State Commun. **138**, 472 (2006).
[11] P. Wartewig, M. K. Krause, P. Esquinazi, S. Rösler, and R. Sonntag, J. Magn. Magn. Mater. **192**, 83 (1999).
[12] W. Zhang, Y. Bai, X. Han, L. Wang, X. Lu, and L. Qiao, J. Alloys Compd. **546**, 234 (2013).
[13] C. J. Li, B. Wang, and J. N. Wang, J. Magn. Magn. Mater. **324**, 1305 (2012).
[14] R. S. Meena, S. Bhattachrya, and R. Chatterjee, J. Magn. Magn. Mater. **322**, 1923 (2010).
[15] G. Shen, Z. Xu, and Y. Li, J. Magn. Magn. Mater **301**, 325 (2006).
[16] P. Enghag, Encyclopedia of The Elements, Wiley-VCH Co., Stockholm (2004) pp. 355-493.
[17] G. Xu, H. Ma, M. Zhong, J. Zhou, Y. Yue, and Z. He, J. Magn. Magn. Mater. **301**, 383 (2006).
[18] M. Montazeri-Pour and A. Ataie, J. Mater. Sci. Technol. **25**, 465 (2009).
[19] P. Xu, X. Han, H. Zhao, Z. Liang, and J. Wang, Mater. Lett. **62**, 1305 (2008).
[20] D. Lisjak and M. Drofenik, J. Eur. Ceram. Soc. **27**, 4515 (2007).
[21] H. Sozeri, Z. Durmuş, A. Baykal, and E. Uysal, J. Mater. Sci. Eng. B **177**, 949 (2012).
[22] A. Ghasemi, A. Hossienpour, A. Morisako, A. Saatchi, and M. Salehi, J. Magn. Magn. Mater. **302**, 429 (2006).
[23] B. H. Toby, J. Appl. Cryst. **38**, 1040 (2005).